Two Redox-Active β-Carotene Molecules in Photosystem II[†]

Cara A. Tracewell and Gary W. Brudvig*

Department of Chemistry, Yale University, P.O. Box 208107, New Haven, Connecticut 06520-8107

Received April 11, 2003; Revised Manuscript Received June 2, 2003

ABSTRACT: Photosystem II (PS II) contains secondary electron-transfer paths involving cytochrome b_{559} (Cyt b_{559}), chlorophyll (Chl), and β-carotene (Car) that are active under conditions when oxygen evolution is blocked such as in inhibited samples or at low temperature. Intermediates of the secondary electron-transfer pathways of PS II core complexes from *Synechocystis* PCC 6803 and *Synechococcus sp.* and spinach PS II membranes have been investigated using low temperature near-IR spectroscopy and electron paramagnetic resonance (EPR) spectroscopy. We present evidence that two spectroscopically distinct redox-active carotenoids are formed upon low-temperature illumination. The Car^+ near-IR absorption peak varies in wavelength and width as a function of illumination temperature. Also, the rate of decay during dark incubation of the Car^+ peak varies as a function of wavelength. Factor analysis indicates that there are two spectral forms of Car^+ (Car_A^+ has an absorbance maximum of 982 nm, and Car_B^+ has an absorbance maximum of 1027 nm) that decay at different rates. In *Synechocystis* PS II, we observe a shift of the Car^+ peak to shorter wavelength when oxidized tyrosine D ($Y_D^\bullet$) is present in the sample that is explained by an electrostatic interaction between $Y_D^\bullet$ and a nearby β-carotene that disfavors oxidation of Car_B. The sequence of electron-transfer reactions in the secondary electron-transfer pathways of PS II is discussed in terms of a hole-hopping mechanism to attain the equilibrated state of the charge separation at low temperatures.

Photosystem II (PS II[1]) is a membrane bound pigment−protein complex that uses light energy to oxidize water to molecular oxygen. The protein complex is composed of D1 and D2 polypeptides, cytochrome b_{559}, the chlorophyll binding proteins CP43 and CP47, several extrinsic membrane bound proteins, and several other small polypeptides whose functions are not well characterized at this time (*1*). Light-harvesting chlorophylls transfer energy to the reaction center primary-donor chlorophyll of PS II (P_{680}), and the charge separation process is initiated. The excited state form of this chlorophyll (P_{680}*) transfers an electron to a nearby pheophytin molecule ($Pheo_A$) (see Figure 1) to generate a charge-separated state (for review, see Diner and Rappaport (*2*)). This state (P_{680}^+−$Pheo^-$) is stabilized by transfer of the electron to the protein bound quinone, Q_A. The electron on Q_A is transferred to Q_B, an exchangeable quinone, which dissociates from PS II upon reduction by two electrons and subsequent transfer of two protons. Under physiological conditions, the oxygen-evolving complex (OEC), containing a tetramanganese cluster, provides electrons from water to reduce the oxidized chlorophyll, P_{680}^+, via a redox-active tyrosine Y_Z. At low temperatures or if the primary electron-transfer pathway to reduce P_{680}^+ is blocked, either in reaction centers where the manganese cluster has fallen out, or has not yet been assembled, then the secondary electron donors of the alternate electron-transfer pathway(s) are oxidized.

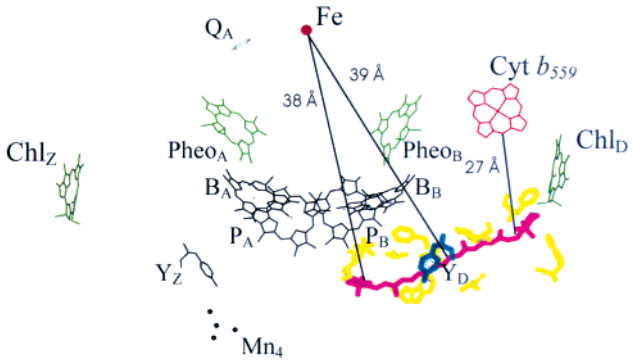

FIGURE 1: The cofactors in the D1/D2 core of PS II together with the cluster of aromatic amino acid residues (yellow) near Y_D (blue), taken from Kamiya and Shen (*18*) (PDB code 1IZL), and a potential location of Car_B (pink) based on this work and Lakshmi et al. (*20*). Distances are shown between the non-heme iron and two atoms of Car_B (38 and 39 Å) and between the heme of Cyt b_{559} and Car_B (27 Å). The edge to edge distance between Y_D and Car is 10 Å and the edge to edge distance between Chl_D and Car is 7 Å.

In *Synechocystis* PS II, the secondary electron donors include Cyt b_{559}, β-carotene (Car), and the redox-active chlorophyll (Chl_Z) that is ligated to His118 in the D1 polypeptide (*3*, *4*). In spinach PS II samples, an additional Chl^+ species was observed, and it was proposed that this species was due to an additional radical cation Chl species,

[†] This work was supported the by DOE, Office of Basic Energy Sciences, Division of Chemical Sciences (DE-FG02-01ER15281), and NIH Predoctoral Traineeship Grant T32 GM008283 (C.A.T.).

* To whom correspondence should be addressed. Phone: (203) 432-5202. Fax: (203) 432-6144. E-mail: gary.brudvig@yale.edu.

[1] Abbreviations: Car, β-carotene; Chl, monomeric chlorophyll; β-DM, β-dodecylmaltoside; Cyt b_{559}, cytochrome b_{559}; D1, D1 polypeptide; D2, D2 polypeptide; EDTA, (ethylenedinitrilo)tetraacetic acid; HPLC, high-pressure liquid chromatography; MES, 2-(*N*-morpholino) ethane sulfonic acid; P_{680}, primary-donor chlorophyll of PS II; PPBQ, phenyl-*p*-benzoquinone; PS II, photosystem II; RC, reaction center; Y_D, redox-active tyrosine 160 of the D2 polypeptide; Y_Z, redox-active tyrosine 161 of the D1 polypeptide.

10.1021/bi0345844 CCC: $25.00
Published on Web 07/11/2003

Chl_D, the Chl ligated to His117 in the D2 polypeptide (*5*). It has been observed that Cyt b_{559}, ultimately, is the electron donor when the heme is reduced by ascorbate (*6*), but in reaction centers where the heme is oxidized, β-carotene (Car^+) and chlorophyll (Chl^+) radical cations are observed. The Car and Chl are described as intermediates in the pathway for Cyt b_{559} oxidation. It has also been shown that Q_B can reduce Cyt b_{559} (*7*). Therefore, the alternate electron donors of PS II have been proposed to participate in cyclic electron transfer in PS II.

Intermediates of the secondary electron-transfer pathways in PS II can be studied by generating the charge-separated state at cryogenic temperatures. At these temperatures, electron transfer from the OEC is blocked because tyrosine oxidation reactions require the movement of protons, which cannot occur in the frozen sample. The initial charge separation in the reaction center produces a quinone radical anion, Q_A^-, and a chlorophyll radical cation, P_{680}^+. Studies suggest that the radical cation hole is located primarily on P_A at low temperatures (5 K) (*8*). The estimated reduction potential of the oxidized primary-donor chlorophyll P_{680}^+ is +1.2 V, but may be as much as 1.4 V (*9*); therefore, it is possible for P_{680}^+ to oxidize nearby β-carotene or chlorophyll molecules in the reaction center. Thermodynamics dictates that the final location of the hole will be the lowest potential donor in the reaction center. However, at low temperatures an energy barrier for additional electron transfer steps may prevent the hole from moving to the lowest potential donor. Therefore, at very low temperatures the hole may be trapped at the species which is kinetically the fastest donor to P_{680}^+. This is indicated in previous work on detergent-solubilized PS II membranes illuminated at 20 K, in which Car^+ was formed initially and upon warming the hole was transferred to a Chl (*10*). In other studies of cyanobacterial PS II core complexes or spinach PS II membranes, illumination at 20 K yielded a mixture of Chl^+ and Car^+ radicals that decayed by charge recombination during dark incubation or warming (*5*).

The cofactors in PS II have been studied extensively. HPLC analysis of pigments extracted from PS II core complexes shows that 38 chlorophylls and ~17 carotenoids are bound to the photosystem II core complex (*11*, *12*). Two β-carotenes are bound to the D1 and D2 polypeptides (*13*), and these are the Car molecules most likely to be close enough to the reaction center Chls to be oxidized. The two β-carotene molecules in the PS II RC have been identified as exclusively all trans-β-carotene using HPLC and resonance Raman spectroscopy (*14*−*16*).

In the first X-ray crystal structure of PS II from *Thermosynechococcus elongatus* (formerly *Synechococcus elongatus*), the positions of 34 chlorin cofactors and two hemes were determined at 3.8 Å resolution (*17*). The heme of Cyt b_{559} is identified in the crystal structure because of its location in the membrane and is nearly 42 Å from P_A, the probable location of P_{680}^+ (*17*, *18*). Such a long distance necessitates an electron-transfer intermediate which has been proposed to be Car and/or Chl (*5*, *10*, *19*). Recently, PS II was crystallized from *Thermosynechococcus vulcanus*, and the structure was solved at 3.7 Å resolution by Kamiya and Shen (*18*). In this structure, an additional chlorophyll was identified in CP43, and two β-carotenes were identified in a region close to the reaction center. The two β-carotene molecules are modeled as having cis and trans configurations, respectively, in the Kamiya and Shen structure and both are in the region of the reaction center between P_A and the heme of Cyt b_{559}. However, the β-ring portions of the cis molecule were not included. The cis carotenoid structure is not consistent with spectroscopic measurements that identify both β-carotenes molecules as all trans, as described above.

Lakshmi et al. (*20*) have proposed a model for the location of the two β-carotenes in PS II based on high-field saturation-recovery EPR distance measurements. The distance measured from Car^+ to the non-heme iron is ~38 Å (*20*). This places the Car^+ species farther from the non-heme iron than modeled in the Kamiya and Shen (*18*) structure. Aromatic residues have been observed to pack around the carotenoid molecules in structurally characterized carotenoid binding proteins (*21*, *22*). Lakshmi et al. (*20*) identified two possible Car-binding sites in the D1/D2 polypeptides where there are clusters of aromatic residues ~38 Å from the non-heme iron. One of the potential Car-binding sites is located near tyrosine D, Y_D (Figure 1).

Differences in the photochemical properties of carotenoids in PS II and the bacterial reaction center give important clues about the location of the carotenoids in PS II. Charge recombination in PS II can result in the formation of the triplet state of P_{680}. Reaction of $^3P_{680}$ with molecular oxygen can lead to the formation of $^1O_2$, a dangerous, highly reactive molecule. β-Carotene can quench $^1O_2$, and this is observed in PS II (*23*). However, another mechanism for quenching ^3Chl is the formation of ^3Car which is observed in bacterial reaction centers. This mechanism requires van der Waals contact of the Car with Chl. ^3Car is not observed in PS II, which suggests that the β-carotene molecules are not in van der Waals contact with the core Chls in PS II. Instead, Car is oxidized when other electron donors cannot reduce P_{680}^+.

Previous studies of the secondary electron-transfer pathways of PS II have proposed linear and branched connectivity between Cyt b_{559} and P_{680}^+ involving Car and/or Chl electron-transfer intermediates (*5*, *10*). Most studies agree that Car is likely the initial donor to P_{680}^+ because Chl_Z is too far from P_{680}^+ for electron transfer to occur in one step and because at low temperatures (20 K) Car^+ is trapped in higher yield than the Chl^+ species, consistent with it being the initial donor to P_{680}^+ (*5*, *10*).

Recent resonance Raman work has shown that two β-carotene molecules bound to PS II reaction center preparations have differences in their electronic and vibrational properties (*24*). The Car^+ species formed in these PS II reaction center preparations can only be formed in the presence of an electron acceptor. This work suggests that the two β-carotene molecules are inequivalent in this protein preparation. On the basis of this work and the presence of only one Cyt b_{559}, it was proposed that only one Car is involved in the cyclic electron-transfer pathway (*19*). An alternate pathway for electron transfer from Chl_Z to P_{680}^+ has been proposed by Vasil'ev et al. (*25*). Their proposal suggests a pathway for Chl_Z oxidation via the Car molecules observed in the Kamiya and Shen structure and several of the Chl cofactors bound to CP43.

As described above, there have been proposals for one or two redox-active Car in PS II, but there is a lack of characterization of Car photooxidation in PS II core complexes. In this paper, we describe evidence for two redox-

active carotenoids that are spectroscopically distinct in PS II core complexes. Oxidation of one of the β-carotene molecules is modulated by the oxidation state of tyrosine D, suggesting that one of the redox-active Car is close to Y_D.

MATERIALS AND METHODS

Chemicals and Reagents. 2-(*N*-Morpholino) ethane sulfonic acid (MES) and β-dodecyl maltoside (β-DM) were purchased from US Biochemicals. Phenyl-*p*-benzoquinone (PPBQ) was purchased from Aldrich and recrystallized twice in ethanol. Stock solutions of PPBQ and potassium ferricyanide (25 mM each) were prepared in DMSO and water, respectively, and frozen until use.

Photosystem II Sample Preparation. PS II samples were prepared from cyanobacteria and spinach. His-tagged PS II core particles were isolated from *Synechocystis* PCC 6803 cells (*26*). *Synechococcus* PS II samples (non-his-tagged) were prepared by purification on an anion exchange DEAE column (*11*). Spinach PS II enriched membranes were isolated from market spinach according to Berthold et al. (*27*).

Photosystem II samples were transferred to a buffer containing 50 mM MES, 15 mM NaCl, 60% (v/v) glycerol at pH 6.0 for all low-temperature measurements. The nonionic detergent β-DM was added to buffers for *Synechocystis* and *Synechococcus* samples at a concentration of 0.03% to maintain the solubilization of the membrane protein. PS II samples were stored at 77 K until use.

Sample Treatments. Mn-depleted PS II samples were prepared by washing into a buffer containing 50 mM MES, 15 mM NaCl, 1 mM $CaCl_2$, 0.4 M sucrose, and 0.03% β-DM (Buffer A). The sample was diluted 1:1 with Buffer A, which also contained 10 mM hydroxylamine and 10 mM Na_2EDTA, and incubated in the dark for 30 min stirring on ice to allow for the reduction of manganese in the tetra-manganese cluster by hydroxylamine. Free manganese was removed by washing with Buffer A that also contained 5 mM Na_2EDTA. Tyrosine D was photooxidized by the following procedure: PPBQ was added to Mn-depleted PS II samples to a final concentration of 500 μM; then samples were incubated in darkness on ice for 30 min, illuminated at room temperature for 30 s to photooxidize Y_D, incubated on ice in the dark for 3 min to allow for any unstable charge separations resulting from Y_Z oxidation to decay, and then frozen.

Near-IR Spectroscopy. A Perkin-Elmer Lambda 20 spectrometer was used to make optical spectroscopic measurements in the near-IR. An Oxford Instruments Optistat liquid helium cryostat was used for measurements between 20 and 140 K. Polyethylene cuvettes with a path length of 1.0 cm were purchased from Fisher and used for low-temperature optical measurements unless otherwise indicated. A 150 W quartz halogen lamp filtered by a 6 in. water bath and a heat-absorbing filter (Schott KG-5) was used to illuminate samples. A fiber optic cable was used to direct the light into the cryostat. Samples were slowly frozen in a liquid nitrogen bath over a period of 15 min to form an optically clear glass. Illuminations were performed on samples that were equilibrated at the specified temperature for at least 60 min or until baseline changes were no longer observed in the spectra of the nonilluminated sample. All light induced spectra were referenced to the dark spectra at the same temperature in order to subtract background absorbance from water. We checked the sample buffer for shifts of the water near-IR bands as a result of the illumination, but we saw no evidence of any change between the dark and illuminated buffer sample.

Frozen samples were illuminated for 15 min inside the cryostat, and data collection was immediately begun. A fresh sample was used for each illumination experiment. Repeated low-temperature illumination spectra were reproducible. However, repeated room-temperature illuminations of the same sample resulted in a reduced yield of radical cations observed in the low-temperature illumination experiments. Extended illumination at room-temperature results in damage to the reaction centers.

EPR Spectroscopy. X-band EPR measurements were made on PS II samples of the sample chlorophyll concentration as the near-IR optical measurements to quantify the level of oxidized tyrosine D. A Varian E-9 EPR spectrometer equipped with a TE_{102} mode cavity and an Oxford Instruments ESR 900 liquid helium cryostat and interfaced to a Macintosh IIci computer was used for measurements at 20 K. X-band EPR conditions were as follows: frequency 9.27 MHz, field modulation frequency 100 kHz, field modulation amplitude 4 G, microwave power 0.02 mW.

Spectral Simulations. SPECFIT/32 was used to perform factor analysis on the near-IR absorption data sets. The program Microcal Origins 6.0 was used to simulate the near-IR absorption data and to analyze the decay kinetics.

RESULTS

Synechocystis, spinach, and *Synechococcus* PS II were dark adapted on ice for at least 2 h before freezing to allow $Y_D^{\bullet}$ to be reduced and then illuminated for 15 min at 20 K. Near-IR spectra of the Car^+ formed are shown in Figure 2. The spectra are scaled to the same absorbance value at the wavelength of maximum absorption (λ_{max}) in order to compare the Car^+ spectral shape. The Car^+ peak position in the *Synechocystis* PS II core complexes is at 984 nm (79 nm wide, full width at half max). The Car^+ spectrum in spinach PS II membranes has a λ_{max} of 996 nm, and the peak is 74 nm in width. Of the three species of PS II examined here, the Car^+ peak width formed in PS II core complexes from the thermophilic cyanobacteria *Synechococcus* is the narrowest (56 nm), and the peak maximum is at the longest wavelength, 998 nm. The variations in the Car^+ electronic spectra of these species may be the combined result of two factors. First, the local protein environment may vary among species. The amino acid sequences of the D1 and D2 polypeptides from these species have been determined, and they are not identical (*28*). Differences of the local protein environments surrounding β-carotene in the reaction centers could produce variations in the solvation of the Car^+, which may result in spectrally distinct Car^+ species (*29*). Second, the reaction center contains two β-carotenes bound to the D1 and D2 polypeptides and there may be more than one oxidized β-carotene molecule contributing to the Car^+ spectrum. The shifts of λ_{max} among species could be explained if there are two spectroscopically distinct Car^+ with species-dependent yields. These results prompted us to study the effects of temperature on the Car^+ spectrum. *Synechocys-*

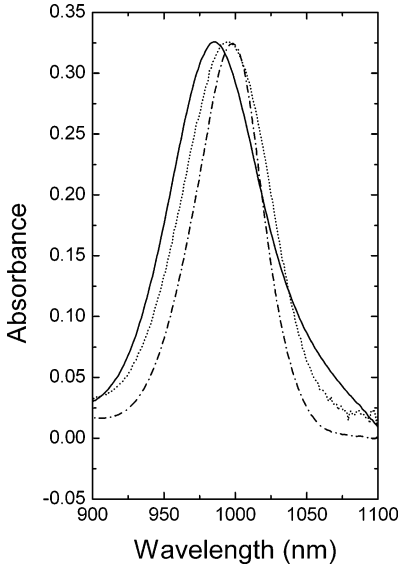

FIGURE 2: Near-IR spectra of Car^+ formed in PS II from three species by 15 min illumination at 20 K after treating the sample with 5 mM potassium ferricyanide to oxidize Cyt b_{559}. Spectra are labeled as follows: O_2-evolving *Synechocystis* PS II core complexes at 2.82 mg/mL (solid), Mn-depleted spinach PS II membranes at 4.68 mg/mL (dotted), and O_2-evolving *Synechococcus* PS II core complexes at 6.29 mg/mL (dash dot). Samples were frozen in plexiglass flatcell with a path length of 1.25 mm. Spinach PS II and *Synechococcus* PS II spectra are scaled by a factor of 1.53 and 0.362, respectively, to compare the spectral characteristics of the Car^+ peak between all samples.

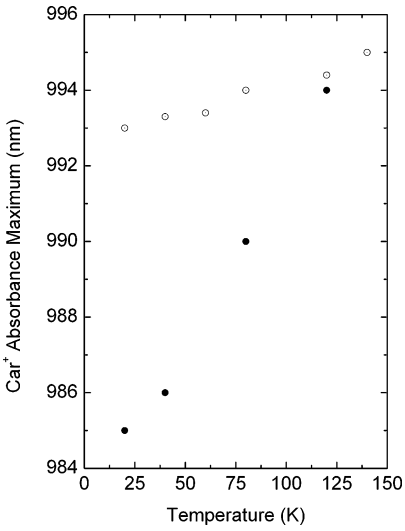

FIGURE 3: Mn-depleted *Synechocystis* PS II Car^+ absorption max varies according to illumination temperature. Chlorophyll sample concentration is 0.30 mg/mL. Solid circles, Car^+ generated by illumination at specified temperature; open circles, Car^+ generated by illumination at 140 K, then cooled to specified temperature.

tis PS II samples were used for these measurements because of the reliability of the sample to form an optical quality glass at low temperature.

The λ_{max} of Car^+ formed in Mn-depleted *Synechocystis* photosystem II as a function of the temperature of sample illumination is shown in Figure 3. The samples were treated with 5 mM potassium ferricyanide prior to being frozen in the dark. After equilibration at a given temperature, the sample was illuminated to generate the $Car^+Q_A^-$ charge separation, and the near-IR absorption was measured at the same temperature. There is a shift in the Car^+ λ_{max} to longer wavelengths at higher illumination temperature. The shift is partly due to the change in temperature of the sample, which causes a shift in the Boltzmann distribution of vibrational states in the ground electronic state. This can be seen in Figure 3 as the λ_{max} for the Car^+ species formed at 140 K shifts to shorter wavelength as the sample is cooled to 20 K. However, the change in the Car^+ peak as a direct function of temperature on the electronic spectrum only accounts for 2−3 nm of the shift. This agrees with the observed spectral shift of neutral β-carotene over these temperatures (*30*). The change in index of refraction upon lowering the temperature alters the polarizability and can shift the absorption spectrum (*31*). This effect manifests as a blue shift in neutral carotenoids. However, the Car^+ peak shifts by nearly 10 nm to the red when the illumination is performed at lower temperature. This result suggests the Car^+ peak may be composed of more than one spectroscopically distinct Car^+ species and the illumination temperature determines the relative yields of the photooxidized species.

Additional evidence for more than one species in the Car^+ peak is observed in the time-evolution of the near-IR spectrum. The decay by charge recombination with Q_A^- in the dark (*5*) of light-induced radical cations formed at 20 K in *Synechocystis* PS II is shown in Figure 4A,B. Near-IR spectra presented in Figure 4A were collected immediately following illumination and approximately 30 min, 4 h, and 10 h after illumination. The Car^+ peak has nearly a Gaussian line shape. However, the spectrum decays at different rates as a function of wavelength. Overall, the decay is multiexponential, having kinetically distinct fast and slow decaying components. In Figure 4B, the absorbance change at two wavelengths (968 and 1011 nm, indicated by arrows in Figure 4A) is plotted as a function of time to illustrate that the rate of decay is not the same at all wavelengths. The absorbance is plotted on a log scale to illustrate the multiexponential behavior of the Car^+ decay. Both fast- and slow-decaying components are present throughout the Car^+ spectrum. Initially, the absorbance value at 968 nm decays more rapidly than at 1011 nm. This results in the shift of the initial Car^+ peak at 986 nm to a longer wavelength, 989 nm, after 10 h of incubation in the dark at 20 K.

We performed factor analysis using the program Specfit32 on 60 near-IR scans collected as a function of dark incubation time at 20 K after the illumination period. Factor analysis can identify the minimum number of spectrally and kinetically distinct components, called factors, in a series of spectra. Five factors were identified, and these are shown in Figure 5A. Primarily, two factors describe the time evolution of the Car^+ spectra (bottom panel). Additional factors (upper panel) describe changes in the Chl^+ region of the spectrum (manuscript in preparation) or are noise. A plot of the relative contribution of the two primary factors to the total spectrum as a function of time is shown in Figure 5B.

The first factor is similar to the Car^+ spectrum, while the second factor has a derivative shape in the Car^+ region of the spectrum. The first factor describes most of the decay of the Car^+ signal. The second factor corrects for the differential decay of the Car^+ peak, which is faster toward the blue side of the peak and slower toward the red side of the peak. We interpret the second factor in the following way: because the decay of the Car^+ peak during dark incubation varies as a function of wavelength, the line shape

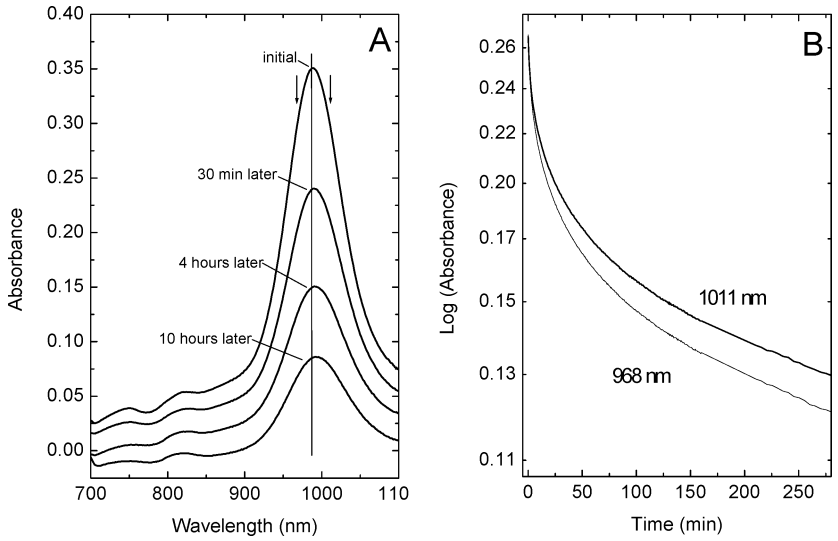

FIGURE 4: (A) Near-IR spectra of *Synechocystis* PS II measured at 20 K showing decay of Car^+ during incubation in the dark (initial, 30 min later, 4 h later, 10 h later). The Car^+ peak maximum shifts from 987 to 989 nm. Chlorophyll concentration of the sample is 0.23 mg/mL. (B) Decay of absorbance at 968 and 1011 nm (indicated by arrows in panel A) as a function of dark incubation time.

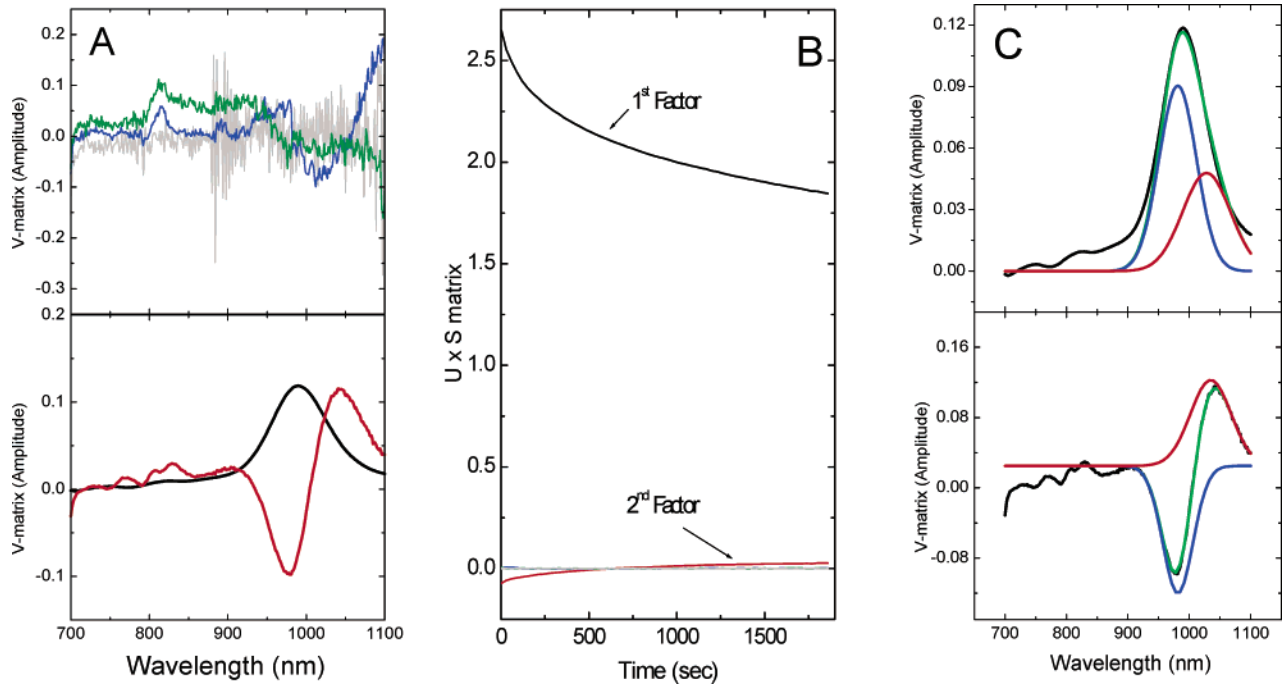

FIGURE 5: (A) Components derived by factor analysis of spectra of *Synechocystis* PS II taken as a function of dark incubation time following illumination at 20 K. (B) Time evolution of Factors. (C) Gaussian fit of Factor 1 (top panel) and Factor 2 (bottom panel) by two Gaussians centered at 982 and 1027 nm having different fixed widths.

of the first factor cannot describe this well. Therefore, the second factor is necessary to reproduce the spectra because it compensates for the differences in the rates of decay. This observation can be explained if there are in fact two spectroscopically distinct Car^+ species that contribute to the Car^+ spectrum.

The first and second factors were fit by two Gaussians (Figure 5C), and the λ_{max} and the peak width values were used to deconvolute spectra of Car^+ generated over a range of illumination temperatures. To differentiate the two simulated Car^+ curves, we will identify the Gaussian centered at the shorter wavelength as Car_A^+ and the Gaussian centered at the longer wavelength as Car_B^+. The shorter-wavelength Gaussian from Car_A^+ is centered at 982 nm and has a narrower peak width of 72 nm, whereas the Gaussian curve from Car_B^+ is centered at 1027 nm and is 92 nm wide. We used the peak positions and widths of these two Gaussian curves to deconvolute the spectra of Car^+ generated by varying the illumination temperature; the spectra were measured immediately after illumination. The deconvoluted Car^+ spectra generated by illumination at 20 and 140 K are shown in Figure 6A,B. A mixture of the two Car^+ species is formed over the range of illumination temperatures studied here. The ratio of maximum absorbance of Car_A^+ at 982 nm over that of Car_B^+ at 1027 nm is plotted as a function of the illumination temperature (Figure 6C). According to the spectral fits, at 140 K the yield of both radical cations is nearly equal. It appears that the Car_A^+ yield is much greater at lower illumination temperature. Car_B^+ formation is slightly larger at warmer illumination temperature, but its yield does

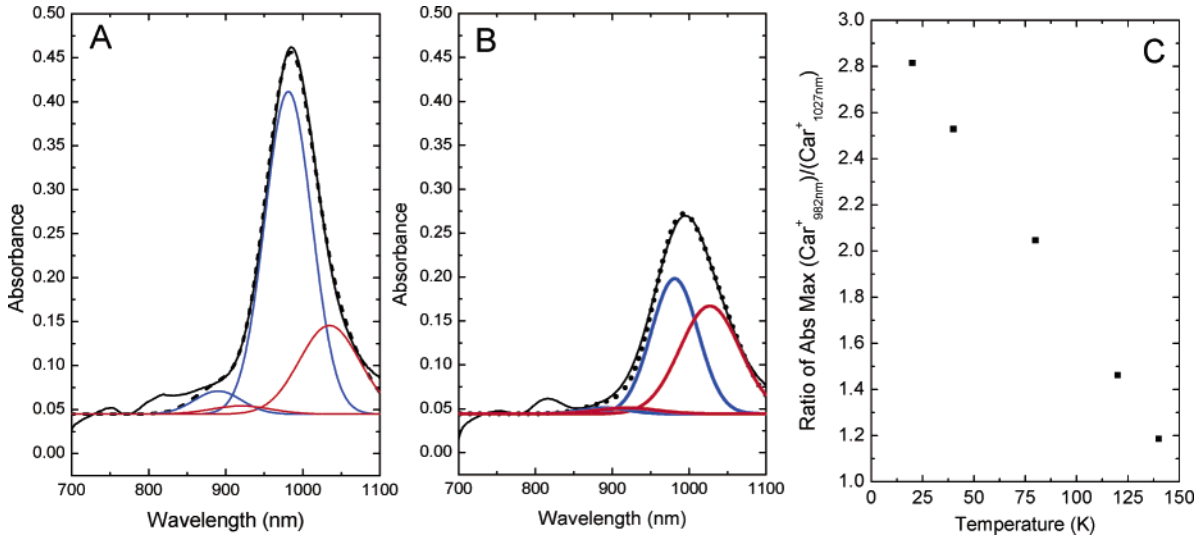

FIGURE 6: Deconvolution of the spectra generated by illumination by using the two Gaussians determined by Factor analysis: (A) 20 and (B) 140 K. Chlorophyll concentration of sample is 0.30 mg/mL. Blue lines: Gaussian curves representing Car_A^+ centered at 982 nm and the Car_A^+ vibronic band centered at 890 nm, width of 72 nm. Red lines: Gaussian curve representing Car_B^+ centered at 1027 nm and the Car_B^+ vibronic band centered at 920 nm, width of 92 nm. Dotted line: sum of Car_A^+ and Car_B^+ main band and vibronic bands. Solid line: near-IR absorbance spectrum. (C) Ratio of the yield of the Car_A^+ to Car_B^+ as a function of illumination temperature.

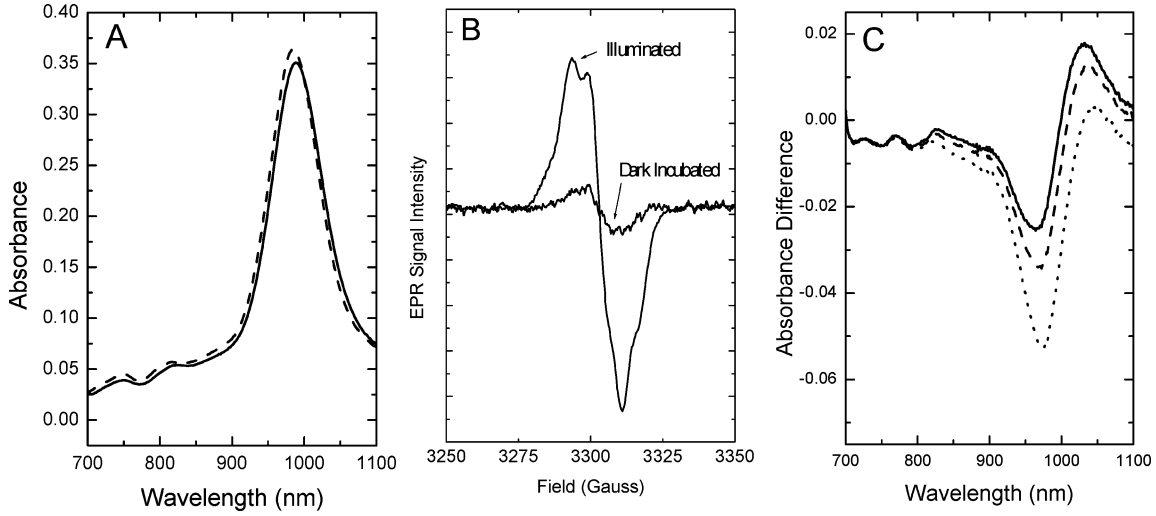

FIGURE 7: (A) Near-IR absorption spectra of Mn-depleted *Synechocystis* PS II showing light-induced signals at 20 K. Solid line, no $Y_D^•$ induced prior to 20 K illumination; dashed line, $Y_D^•$ induced prior to illumination (see methods for $Y_D^•$ generation protocol). Chlorophyll concentration in the sample is 0.30 mg/mL. (B) EPR signals from the sample used in part A. Sample treatments are indicated. (C) Near-IR difference of the spectra shown in part A (solid line) and spectra measured after dark incubation; dashed line, difference 1 min later; dotted line, difference 10 min later.

not vary as much as Car_A^+ over the temperature range studied. The two Car^+ species decay at different rates, and also both species appear to have a fast and a slow decaying component.

Previous proposals have suggested that the two β-Car in D1/D2 are bound in symmetric positions in D1 and D2, respectively (*12*, *19*). Recently, Lakshmi et al. suggested symmetric binding of the Car molecules in the reaction center with one Car molecule in a binding pocket near tyrosine D (*20*), the redox-active residue located in the D2 polypeptide. Alternatively, Kamiya and Shen present a model in which both β-carotenes are located on the D2 side of the reaction center, that is, between P_{680} and Cyt b_{559} (*18*); the modeled trans and *cis*-β-carotene molecules are located 25.7 and 32.7 Å, respectively, from Y_D (*18*). To test these proposals, we have examined the effect of the redox state of Y_D on Car^+ formation. Diner et al. observe an electrochromic effect from oxidized Y_D ($Y_D^•$) on the absorbance spectrum of P_{680} (*2*). Faller et al. have recently suggested that the P_{680}^+ reduction rate by Y_Z is slower in the presence of Y_D than $Y_D^•$ (*32*) owing to an electrostatic interaction from $Y_D^•$ that shifts the location of the cation to reside on P_A (the closest Chl toY_Z). On the basis of these results, it is possible that oxidation of Y_D would modulate the yield of Car^+ if one of the β-carotenes is close to Y_D.

The effect of tyrosine D oxidation on Car^+ formation in Mn-depleted *Synechocystis* PS II samples is shown in Figure 7. The EPR spectra of a *Synechocystis* PS II sample before and after room-temperature illumination are shown in Figure 7B. The yield of $Y_D^•$ in each EPR spectrum was measured by double integration of the radical spectrum. The yield of $Y_D^•$ is assumed to be 1 radical per PS II in samples where the radical was induced by illumination at room temperature for 30 s followed by dark incubation for 3 min and rapid

freezing in liquid nitrogen. Note that in the experiments described above, we studied Car^+ yields in dark-adapted PS II. Under these conditions, samples contained $Y_D^\bullet$ in about 10% of the reaction centers.

As shown in Figure 7A, the entire Car^+ spectrum shifts to shorter wavelength when Y_D is oxidized. The rate of Car^+ decay in a sample containing $Y_D^\bullet$ is also different from that in the sample containing mostly Y_D. This is illustrated in Figure 7C. We subtracted the initial spectrum of the sample containing $Y_D^\bullet$ from the initial spectrum of PS II containing mostly Y_D (solid line). Also shown are the difference spectra after 1 min (dashed) and 10 min (dotted) of dark incubation at 20 K. The temporal evolution of the difference spectra shows that the Car^+ spectrum decays at different rates as a function of wavelength and these rates are affected by the presence of $Y_D^\bullet$ in the sample. The difference spectra in Figure 7C also show that $Y_D^\bullet$ affects the relative yields of Chl^+ and will be described in further detail in a forthcoming manuscript.

DISCUSSION

Illumination of PS II core complexes at temperatures from 20 to 140 K generates a charge separation in which Chl^+ and Car^+ are formed. The Car^+ near-IR absorption spectrum shifts 10 nm to longer wavelengths when the illumination temperature is 140 K relative to 20 K in *Synechocystis* PCC 6803 PS II. Only 2−3 nm of the shift can be attributed to a shift in the Boltzmann distribution of vibrational states as a function of temperature (Figure 3). On the basis of the results of factor analysis, we conclude there are two spectroscopically distinct Car^+ species contributing to the Car^+ near-IR spectrum. The observed shift in the Car^+ near-IR absorption spectrum as a function of illumination temperature is due to a change in proportion of each Car^+ species formed. The contribution of each Car^+ to the near-IR spectrum depends on the temperature of the sample during illumination. Car_A^+ is formed in significantly higher yield at low temperatures than Car_B^+, whereas the yield of Car_B^+ is somewhat higher at 140 K than at 20 K. Differences in the two Car^+ species are also apparent in their stability during dark incubation. Car_A^+ species is less stable than Car_B^+ at 20 K. Because the total yield of Car^+ radicals is lower at 140 K than 20 K, it is likely that the lower yield of Car_A^+ at 140 K is due to its decay before the near-IR spectrum was recorded. The differential stability of Car_B^+ and Car_A^+ may be related to the distance between each of these Car^+ species and Q_A or P_A.

We hypothesize that the protein environment surrounding the Car molecule may affect the observed Car^+ near-IR spectrum. Differences in the local environment surrounding each β-carotene molecule in the protein could produce spectroscopically distinct Car^+. Measurements of Car^+ cation radicals formed by pulsed radiolysis in polar and apolar solvents demonstrate a dependence of the Car^+ absorbance maximum on the solvation environment (*33*, *34*). Therefore, the local dielectric is expected to influence the Car^+ spectrum. In the protein, differences in the local dielectric could matriculate through π-stacking interactions of the Car polyene chain with the aromatic amino acids, and local dipoles or charges of amino acids. The variations of Car^+ spectral properties formed in PS II among the three organisms

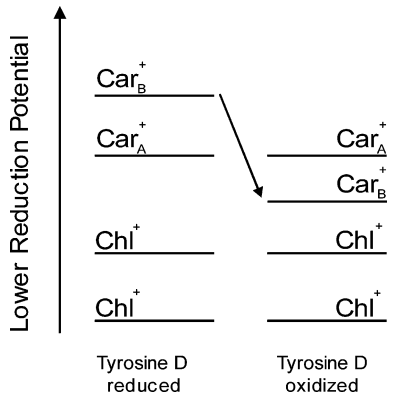

FIGURE 8: Model for changes in the reduction potential of Car_B^+ as a function of Y_D oxidation.

(Figure 2) may reflect differences in the protein environment of the radical cation in each of these reaction centers. For example, the variations in line width of the Car^+ peak may reflect heterogeneity of Car^+ molecular structure in the protein or heterogeneity in Car−protein interactions. Twisting of the polyene breaks the π-conjugation, resulting in altered electronic properties of Car^+ (*19*). However, it is also possible that the differences are related to the number of Car molecules oxidized in each reaction center. In this case, the narrower line width of the Car^+ peak observed in *Synechococcus* PS II compared to *Synechocystis* PS II may reflect formation of only one Car^+ in the former sample.

It is apparent that oxidation of Y_D has an effect on the Car^+ near-IR absorption spectrum (Figure 7A) by the blue shift of the Car^+ peak in PS II core complex samples containing $Y_D^\bullet$ with respect to dark-adapted PS II. The results of Faller et al. (*32*) and Diner et al. (*2*) indicate that oxidized Y_D has electrostatic properties. We consider two possible ways in which a positive charge on or in the vicinity of the oxidized tyrosine D may affect the near-IR spectrum of the Car^+.

First, an electrostatic interaction of the positive charge near $Y_D^\bullet$ with Car^+ may result in an electrochromic shift of the Car^+ peak. For this to occur, the positive charge must be close enough to interact with the Car^+ molecule, and this could result in a shift in the energy of either the ground or excited electronic state of Car^+ species. A shift in the energy difference of these levels would be apparent as a shift in the Car^+ electronic spectrum. However, such a shift would be apparent in a difference spectrum as a derivative shaped feature. While this is what is observed in the spectrum taken immediately after illumination (Figure 7C, solid line), spectra taken after dark incubation are not consistent with an electrochromic shift because these difference spectra show that only one lobe of the derivative line shape changes with time.

Second, the effect of $Y_D^\bullet$ formation on the Car^+ spectrum can be interpreted in the context of the two spectrally distinct Car^+ species. The positive charge on or near $Y_D^\bullet$ may affect Car^+ formation by decreasing the probability that the Car near Y_D will be oxidized as a result of electrostatic repulsion. A positive charge near the Car would increase the reduction potential of this Car^+ molecule making it more difficult to oxidize (Figure 8). If this occurs for one Car molecule and not the other, then the relative proportions of two spectroscopically distinct Car^+ will change, and the absorption peak

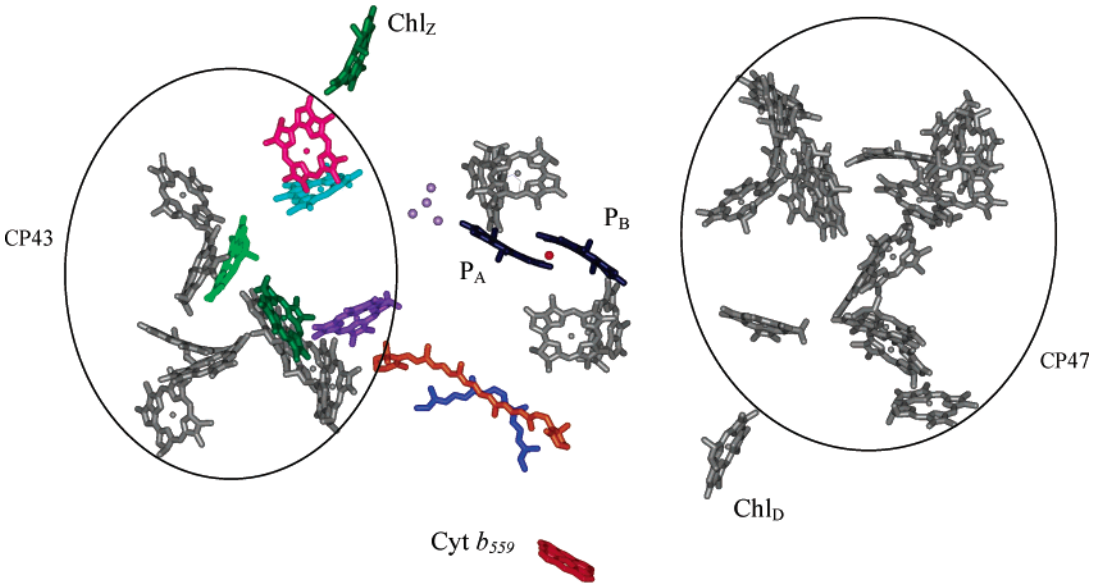

FIGURE 9: Cofactors of PS II as modeled in the Kamiya and Shen PS II (*18*) structure (PDB ID code 1IZL). Circles enclose the Chl cofactors in CP43 and CP47. Chlorophyll molecules in CP43 which may be part of an electron-transfer pathway for Chl$_Z$ oxidation are indicated in color.

position will shift. In the near-IR spectrum of $Y_D^{\bullet}$-containing PS II, the Car^+ peak shifts to shorter wavelengths because less Car_B^+ is formed, and also more Car_A is oxidized. This interpretation can also explain the differences in the decay of the Car^+ in the presence of $Y_D^{\bullet}$ (Figure 7 C). These results provide strong support for one of the Car molecules being located closer to Y_D than the other.

A model for the locations of two Car molecules was presented in the recent X-ray crystallographic structure of PS II (*18*) and is shown in Figure 9. Neither Car molecule is located in the region of the RC analogous to the spheroidene binding site in the purple bacterial reaction center. Both Car molecules in the Kamiya and Shen (*18*) structure are nearly parallel to the membrane plane and are on the outer perimeter of the D1 polypeptide transmembrane helices, in a region between P_{680} and Cyt b_{559}. Portions of both molecules extend into the protein−lipid interface where the D1 polypeptide interacts with the VI helix of CP43 and two other transmembrane polypeptides assigned to psbI and psbK. The assignment of one *cis*-Car molecule in the 3.7 Å resolution PS II structure is surprising because characterization of β-carotene stereochemistry reported for D1/D2/Cyt b_{559} preparations has identified two all *trans*-β-carotenes (*14*−*16*). At 3.7 Å resolution, distinguishing between the electron density of chlorophyll phytyl tails, lipids, and Car molecules may be difficult. The closest edge-to-edge distance from tyrosine D to the *trans*-Car is 25.7 Å and to the *cis*-Car is 32.7 Å (*18*). If the radical cation is located on either of the two Car molecules in the Kamiya and Shen structure, then it is not immediately clear how tyrosine oxidation could exert a significant electrostatic interaction over these long distances.

In the Kamiya and Shen structure, the center-to-center distances from the *trans*-Car and the *cis*-Car to the non-heme iron are 25 and 21 Å, respectively. However, saturation-recovery W-band EPR distance measurements predict that Car^+ is 38 Å from the non-heme iron (*20*). Carotenoid molecules bind to proteins by packing with the hydrophobic amino acids such as tryptophan, phenylalanine, or tyrosine as observed in the structure of the LH−II complex from *Rhodospirillum molischianum* (*21*). On the basis of two clusters of these amino acids in the PS II structure approximately 38 Å from the non-heme iron, Lakshmi et al. (*20*) proposed a model for the location of the two β-carotenes in PS II; one of the Car-binding sites is adjacent to Y_D. The Car-binding site near Y_D, together with the cluster of aromatic amino acids, is shown in Figure 1. On the basis of our spectroscopic evidence, we propose Car_B is the molecule close to Y_D in the D2 protein. Under the conditions of the saturation-recovery EPR measurements of Lakshmi et al. (*20*), there is more of the stable carotenoid radical cation, Car_B^+, present in the sample. As a result, the distance measured by Lakshmi et al. (*20*) should correspond to the Car_B^+-non-heme iron distance. Thus, our present results are consistent with those of Lakshmi et al. (*20*) and together provide evidence for the more stable Car_B^+ being located near $Y_D^{\bullet}$ at a distance of ~38 Å from the non-heme iron.

The location of the less stable Car_A^+ is not as clear. One possibility is that Car_A maybe located in the D1 protein in a symmetry-related position to the Car-binding site near Y_D, as suggested in previous studies (*19*, *20*). Alternatively, Car_A may be in the position of the all-trans Car molecule in the Kamiya and Shen model (*18*). Because the all-trans Car modeled in the Kamiya and Shen (*18*) structure is only ~25 Å from the non-heme iron, if the radical cation is located on the all-trans Car molecule, it would have to be the less stable Car^+ in order to be consistent with the results of Lakshmi et. al (20). Both of these models place the Car molecules closer to P_A than the distance of Chl$_Z$/Chl$_D$ to P_A. This agrees with several experimental observations of the system for formation and decay of the Car^+ and Chl^+ radical cations which indicate that Car is an earlier electron donor than Chl$_Z$/Chl$_D$. These models also suggest that one Car molecule is close to Y_D and the other further away, which agrees well with our present results.

The model shown in Figure 1 places the redox-active Chl and Car molecules adjacent to each other and to Cyt b_{559}, which would allow for rapid electron transfer among the

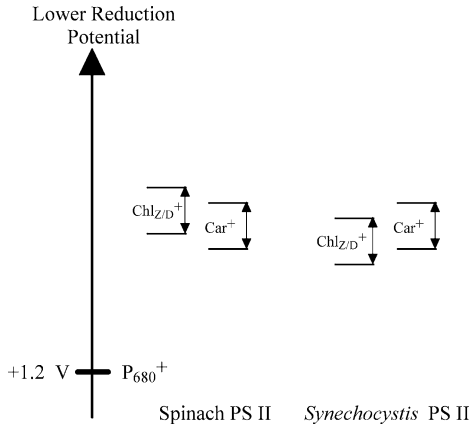

FIGURE 10: Model of reduction potentials for the secondary electron transfer donors of photosystem II. Chl and Car have reduction potentials of 0.78 and 1.1 V, respectively, measured in vivo (*35*, *36*). In the protein environment, the reduction potentials are expected to shift as a result of solvation and to exhibit a distribution of values in frozen samples.

secondary electron-transfer pathway intermediates. Besides the distance between the secondary electron-transfer pathway intermediates, another important factor that determines the rates of electron transfer is the relative redox potential of these molecules. Good spatial connectivity between the intermediates allows the hole to migrate between the centers to the lowest potential redox center. This explains why Cyt b_{559} is the preferential donor when the heme is reduced. In this case, the hole moves to the heme because it is the lowest potential redox center. But if Cyt b_{559} is oxidized, as it is in this study, then we observe a heterogeneous population of oxidized species. This occurs because the redox potentials for the Car^+ and Chl^+ molecules bound to the protein are all relatively close. The reduction potential of β-Car^+ measured in micelles is 1.06 V (*35*). The simulated lipid environment of the micelle is similar to the hydrophobic environment of the β-carotene molecules in PS II. The reduction potential of Chl^+ in solvent is 0.78 V, but in the hydrophobic environment of the protein, this value is probably higher (*36*, *37*). Reduction potentials for both Car^+ and Chl^+ molecules will likely depend on the solvation provided by the protein matrix resulting in a range of values. The lowest potential center in a sample of PS II reaction centers is not homogeneous because freezing the sample traps a distribution of conformers, which yields a distribution of redox potentials of Car and Chl. Figure 10 illustrates a model for the relative reduction potentials of the secondary electron donors in PS II. Both Car^+ and Chl^+ are observed in *Synechocystis* PS II core complexes and spinach PS II membranes samples (*5*). The observation that relatively more Chl^+ is formed in spinach PS II membranes relative to *Synechocystis* PS II core complexes can be explained by a shift in the distribution of Chl^+ and Car^+ reduction potentials in the two species. From these studies, it was hypothesized that hole hopping to the lowest potential center may occur in PS II reaction centers (*38*).

Previous studies of the secondary electron-transfer pathways of PS II have been concerned with the connectivity of Cyt b_{559} to P_{680}. Linear and branched pathways through Car or Car and Chl were proposed (*5*, *10*). The observation of two spectroscopically distinct Car molecules here and in Telfer et al. (*24*), and our observation that one of these Car molecules is in close proximity to Y_D while the other is not, suggests that more than one pathway exists. The structure of β-carotene lends itself to the hole hopping mechanism in that it can act as a molecular wire, connecting the centrally located oxidizing species, P_{680}^+, to move the hole to the peripheral chlorophylls of the reaction center. Vasil'ev et al. (*25*) suggest a mechanism for Chl_Z oxidation based on the locations of Car and Chl molecules in the Kamiya and Shen (*18*) PS II crystal structure. The Car molecules modeled in the reaction center are in close contact with a few of the Chl molecules bound to CP43 and these Chls are part of a Chl chain in CP43. The additional Chl identified in CP43 in the Kamiya and Shen (*18*) structure connects the Chl molecules of CP43 to Chl_Z. The close connectivity of these cofactors implicates a pathway for electron transfer from the Car molecules bound on the D2 side to Chl_Z on the D1 side through the chain of CP43 Chl molecules. This suggests that several redox-active Chl molecules may function in the secondary electron-transfer pathways, in addition to the two redox-active Car molecules identified in this study.

REFERENCES

1. Debus, R. J. (2000) *Metal Ions Biol. Syst. 37*, 657−711.
2. Diner, B. A., and Rappaport, F. (2002) *Annu. Rev. Plant Biol. 53*, 551−580.
3. Stewart, D. H., Cua, A., Chisholm, D. A., Diner, B. A., Bocian, D. F., and Brudvig, G. W. (1998) *Biochemistry 37*, 10040−10046.
4. Stewart, D. H., and Brudvig, G. W. (1998) *Biochim. Biophys. Acta 1367*, 63−87.
5. Tracewell, C. A., Cua, A., Stewart, D. H., Bocian, D. F., and Brudvig, G. W. (2001) *Biochemistry 40*, 193−203.
6. de Paula, J. C., Innes, J. B., and Brudvig, G. W. (1985) *Biochemistry 24*, 8114−8120.
7. Buser, C. A., Diner, B. A., and Brudvig, G. W. (1992) *Biochemistry 31*, 11449−11459.
8. Diner, B. A., Schlodder, E., Nixon, P. J., Coleman, W. J., Rappaport, F., Lavergne, J., Vermaas, W. F. J., and Chisholm, D. A. (2001) *Biochemistry 40*, 9265−9281.
9. Rappaport, F., Guergova-Kuras, M., Nixon, P. J., Diner, B. A., and Lavergne, J. (2002) *Biochemistry 41*, 8518−8527.
10. Hanley, J., Deligiannakis, Y., Pascal, A., Faller, P., and Rutherford, A. W. (1999) *Biochemistry 38*, 8189−8195.
11. Tang, X. S., and Diner, B. A. (1994) *Biochemistry 33*, 4594−4603.
12. Tracewell, C. A., Vrettos, J. S., Bautista, J. A., Frank, H. A., and Brudvig, G. W. (2001) *Arch. Biochem. Biophys. 385*, 61−69.
13. Bassi, R., Pineau, B., Dainese, P., and Marquardt, J. (1993) *Eur. J. Biochem. 212*, 297−303.
14. Fujiwara, M., Hayashi, H., Tasumi, M., Kanaji, M., Koyama, Y., and Satoh, K. (1987) *Chem. Lett. 10*, 2005−2008.
15. Yruela, I., Tomas, R., Sanjuan, M. L., Torrado, E., Aured, M., and Picorel, R. (1998) *Photochem. Photobiol. 68*, 729−737.
16. Ghanotakis, D. F., de Paula, J. C., Demetriou, D. M., Bowlby, N. R., Petersen, J., Babcock, G. T., and Yocum, C. F. (1989) *Biochim. Biophys. Acta 974*, 44−53.
17. Zouni, A., Witt, H. T., Kern, J., Fromme, P., Krauss, N., Saenger, W., and Orth, P. (2001) *Nature 409*, 739−743.
18. Kamiya, N., and Shen, J. R. (2003) *Proc. Natl. Acad. Sci. U.S.A. 100*, 98−103.
19. Telfer, A. (2002) *Philos. Trans. R. Soc. London, Ser. B 357*, 1431−1439.
20. Lakshmi, K. V., Poluektov, O. G., Reifler, M. J., Wagner, A. M., Thurnauer, M. C., and Brudvig, G. W. (2003) *J. Am. Chem. Soc. 125*, 5005−5014.
21. Koepke, J., Hu, X. C., Muenke, C., Schulten, K., and Michel, H. (1996) *Structure 4*, 581−597.
22. Deisenhofer, J., Epp, O., Miki, K., Huber, R., and Michel, H. (1985) *Nature 318*, 618−624.
23. Telfer, A., Dhami, S., Bishop, S. M., Phillips, D., and Barber, J. (1994) *Biochemistry 33*, 14469−14474.
24. Telfer, A., Frolov, D., Barber, J., Robert, B., and Pascal, A. (2003) *Biochemistry 42*, 1008−1015.

25. Vasil'ev, S., Brudvig, G. W., and Bruce, D. (2003) *FEBS Lett. 543*, 159−163.
26. Lakshmi, K. V., Reifler, M. J., Chisholm, D. A., Wang, J. Y., Diner, B. A., and Brudvig, G. W. (2002) *Photosynth. Res. 72*, 175−189.
27. Berthold, D. A., Babcock, G. T., and Yocum, C. F. (1981) *FEBS Lett. 134*, 231−234.
28. Svensson, B., Vass, I., and Styring, S. (1991) *Z. Naturforsch. 46c*, 765−776.
29. Edge, R., and Truscott, T. G. (1999) in *Advances in Photosynthesis: The Photochemistry of Carotenoids* (Frank, H. A., Young, A. J., Britton, G., and Cogdell, R. J., Eds.) pp 223−243, Kluwer Academic Publishers, Dordrecht, The Netherlands.
30. Renge, I., van Grondelle, R., and Dekker, J. P. (1996) *J. Photochem. Photobiol. A 96*, 109−121.
31. Andersson, P. O., Gillbro, T., Ferguson, L., and Cogdell, R. J. (1991) *Photochem. Photobiol. 54*, 353−360.
32. Faller, P., Debus, R. J., Brettel, K., Sugiura, M., Rutherford, A. W., and Boussac, A. (2001) *Proc. Natl. Acad. Sci. U.S.A. 98*, 14368−14373.
33. Edge, R., Land, E. J., McGarvey, D., Mulroy, L., and Truscott, T. G. (1998) *J. Am. Chem. Soc. 120*, 4087−4090.
34. Hill, T. J., Land, E. J., McGarvey, D. J., Schalch, W., Tinkler, J. H., and Truscott, T. G. (1995) *J. Am. Chem. Soc. 117*, 8322−8326.
35. Edge, R., Land, E. J., McGarvey, D. J., Burke, M., and Truscott, T. G. (2000) *FEBS Lett. 471*, 125−127.
36. Blankenship, R. E., and Prince, R. C. (1985) *Trends Biochem. Sci. 10*, 382−383.
37. Thompson, L. K., and Brudvig, G. W. (1988) *Biochemistry 27*, 6653−6658.
38. Tracewell, C. A., and Brudvig, G. W. (2001) *PS2001 Proceedings: 12th International Congress on Photosynthesis*, S5-001, CSIRO Publishing, Melbourne, Australia (http://www.publish.csiro.au/ps2001, accessed Sept 2001).

BI0345844